TIDE-TSUNAMI INTERACTIONS

Zygmunt Kowalik, Tatiana Proshutinsky,
Institute of Marine Science, University of Alaska, Fairbanks, AK, USA

Andrey Proshutinsky,
Woods Hole Oceanographic Institution, Woods Hole, MA, USA

ABSTRACT

In this paper we investigate important dynamics defining tsunami enhancement in the coastal regions and related to interaction with tides. Observations and computations of the Indian Ocean Tsunami usually show amplifications of the tsunami in the near-shore regions due to water shoaling. Additionally, numerous observations depicted quite long ringing of tsunami oscillations in the coastal regions, suggesting either local resonance or the local trapping of the tsunami energy. In the real ocean, the short-period tsunami wave rides on the longer-period tides. The question is whether these two waves can be superposed linearly for the purpose of determining the resulting sea surface height (SSH) or rather in the shallow water they interact nonlinearly, enhancing/reducing the total sea level and currents. Since the near–shore bathymetry is important for the run-up computation, Weisz and Winter (2005) demonstrated that the changes of depth caused by tides should not be neglected in tsunami run-up considerations. On the other hand, we hypothesize that much more significant effect of the tsunami-tide interaction should be observed through the tidal and tsunami currents. In order to test this hypothesis we apply a simple set of 1-D equations of motion and continuity to demonstrate the dynamics of tsunami and tide interaction in the vicinity of the shelf break for two coastal domains: shallow waters of an elongated inlet and narrow shelf typical for deep waters of the Gulf of Alaska.

1. EQUATION OF MOTION AND CONTINUITY FOR THE TSUNAMI-TIDE INTERACTION.

The tide-tsunami interaction will be investigated based on the long-wave equations of motion (Kowalik and Proshutinsky, 1994)

$$\frac{\partial u}{\partial t} + u\frac{\partial u}{\partial x} + v\frac{\partial u}{\partial y} - fv = -g\frac{\partial \zeta}{\partial x} - \frac{\partial \Omega_T}{\partial x} - \tau_x^b/\rho D \tag{1}$$

$$\frac{\partial v}{\partial t} + u\frac{\partial v}{\partial x} + v\frac{\partial v}{\partial y} + fu = -g\frac{\partial \zeta}{\partial y} - \frac{\partial \Omega_T}{\partial y} - \tau_y^b/\rho D \tag{2}$$

In these equations: x and y are coordinates directed towards East and North, respectively; velocities along these coordinates are u and v; t is time; Coriolis parameter $f = 2\Omega\sin\phi$ is a function of the Earth's angular velocity $\Omega = 7.29\times10^{-5}\,s^{-1}$ and the latitude - ϕ; ρ denotes density of the sea water; ζ is the sea level change around the mean sea level; Ω_T is the tide producing potential, and τ_x^b and τ_y^b are components of the stress at the bottom; $D = H + \zeta$ is the total depth equal to the average depth H plus the sea level variations ζ. The bottom stress is proportional to the square of the velocity:

$$\tau_x^b = \rho r u\sqrt{u^2 + v^2} \qquad \text{and} \qquad \tau_y^b = \rho r v\sqrt{u^2 + v^2} \tag{3}$$

The dimensionless friction coefficient r is taken as $r = 2.6\times10^{-3}$.
Equation of continuity for the tsunami-tide problem is formulated as,

$$\frac{\partial}{\partial t}(\zeta - \zeta_b) + \frac{\partial uD}{\partial x} + \frac{\partial vD}{\partial y} = 0 \tag{4}$$

Here, D is the total depth defined as $D = H + \zeta - \zeta_b$, ζ as before denotes the free surface change and ζ_b is the bottom deformation.
The tidal potential in eqs.1 and 2 is related to the equilibrium tides. It is given by the equilibrium surface elevation (ζ_0) as (Pugh, 1987)

$$\zeta_0 = -\frac{\Omega_T}{g} \tag{5}$$

Harmonic constituents of the equilibrium tide can be represented in the following way:
Semidiurnal species

$$\zeta_0 = K\cos^2\phi\cos(\omega t + \kappa + 2\lambda) \tag{6}$$

Here: K – amplitude (see Table 1), ϕ – latitude, ω - frequency, κ – astronomical argument, λ – longitude (east)
Diurnal species

$$\zeta_0 = K\sin 2\phi\cos(\omega t + \kappa + \lambda) \tag{7}$$

Long-period species

$$\zeta_0 = K(\frac{3}{2}\cos^2\phi - 1)\cos(\omega t + \kappa) \tag{8}$$

The amplitude factor K gives magnitude of the individual constituents in the total sea level due to equilibrium tide. The strongest constituent is M_2 with amplitude 0.24 m, the next constituent K_1 of mixed luni-solar origin has amplitude 0.14 m.

TABLE 1. PARAMETERS OF THE MAJOR TIDAL CONSTITUENTS

Name of tide	Symb	Period	Freq. (s^{-1})-ω	K Ampl. (m)
Semidiurnal Species				
Principal Lunar	M_2	12.421h	$1.40519 \cdot 10^{-4}$	0.242334
Principal Solar	S_2	12.000h	$1.45444 \cdot 10^{-4}$	0.112841
Elliptical Lunar	N_2	12.658h	$1.37880 \cdot 10^{-4}$	0.046398
Declination Luni-Solar	K_2	11.967h	$1.45842 \cdot 10^{-4}$	0.030704
Diurnal Species				
Declination Luni-Solar	K_1	23.934h	$0.72921 \cdot 10^{-4}$	0.141565
Principal lunar	O_1	25.819h	$0.67598 \cdot 10^{-4}$	0.100574
Principal solar	P_1	24.066h	$0.72523 \cdot 10^{-4}$	0.046843
Elliptical lunar	Q_1	26.868h	$0.64959 \cdot 10^{-4}$	0.019256
Long-Period Species				
Fortnightly Lunar	Mf	13.661d	$0.053234 \cdot 10^{-4}$	0.041742
Monthly Lunar	Mm	27.555d	$0.026392 \cdot 10^{-4}$	0.022026
Semiannual Solar	Ssa	182.621d	$0.0038921 \cdot 10^{-4}$	0.019446

2. ONE-DIMENSIONAL MOTION IN A CHANNEL.

Above equation we apply first for one-dimensional channel with the bathymetric cross-section corresponding to the typical depth distribution in the Gulf of Alaska (Fig. 1). The algorithm for the run-up in a channel is taken from Kowalik et. al., (2005).

At the right boundary a run-up algorithm was applied. At the left open boundary, a radiation condition based on the known tidal amplitude and current is prescribed (Flather, 1976; Durran, 1999; Kowalik, 2003).

The value of an invariant along incoming characteristic to the left boundary is defined as $(\zeta_p + u_p\sqrt{H/g})/2$ and for the smooth propagation into domain this value ought to be equal to the invariant specified inside computational domain in the close proximity to the boundary $(\zeta + u\sqrt{H/g})/2$. This yield equation for the velocity to be specified at the left boundary as

$$u = u_p - \sqrt{g/H}(\zeta - \zeta_p) \qquad (9)$$

In this formula ζ_p and u_p are prescribed tidal sea level and velocity. For one tidal constituent the sea level and velocity can be written as amplitude and phases of a periodical function:

$$\zeta_p = z_{amp} \cos(\omega t - z_{phase}) \quad \text{and} \quad u_p = u_{amp} \cos(\omega t - u_{phase}) \qquad (10)$$
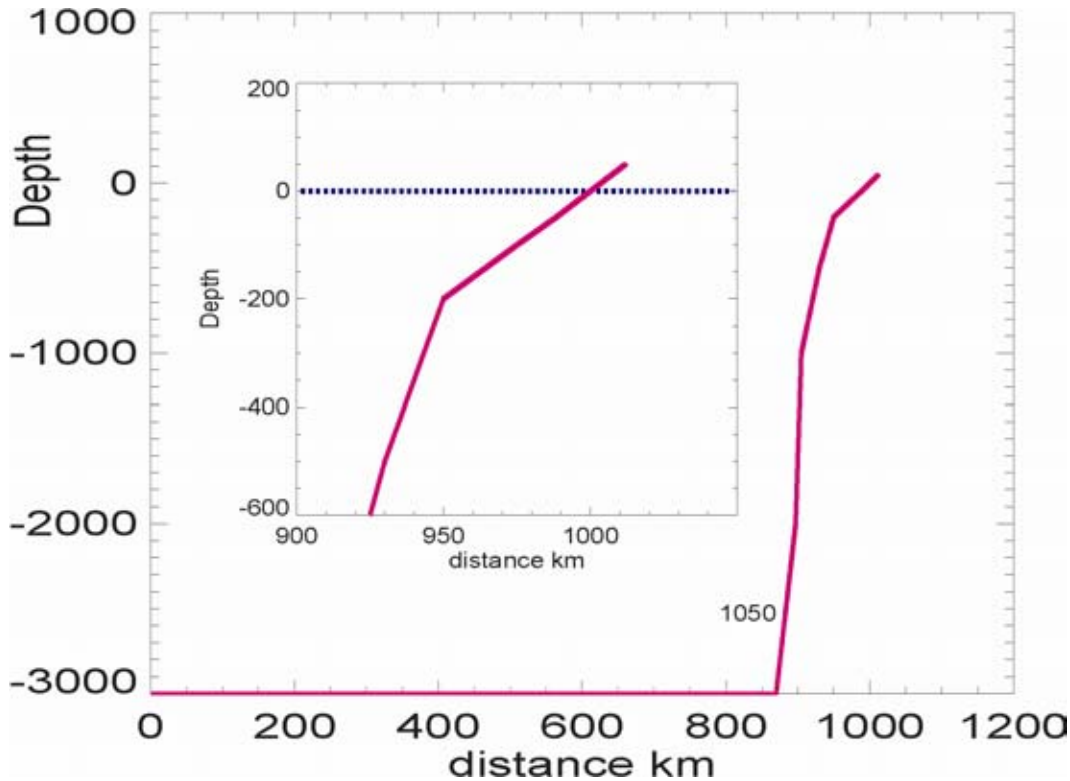
Here ω is a frequency given in Table 1.

Figure 1. Typical bathymetry (in meters) profile cutting continental slope and shelf break in the Gulf of Alaska. Inset shows shelf and sloping beach.

We start computation by considering tsunami generated by an uniform bottom uplift at the region located between 200 and 400km of the 1-D canal from Fig. 1. Short-period tsunami waves require the high spatial and temporal resolution to reproduce runup and the processes taking place during the short time of tide and tsunami interaction. The space step is taken as 10m
As no tide is present in eq. (9) prescribed tidal sea level and velocity are set to zero.
In Figure 2, a 2m tsunami wave mirrors the uniform bottom uplift occurring at 40s from the beginning of the process Later, this water elevation splits into two waves of 1m height each traveling in opposite directions (T=16.7min). While the wave, traveling towards the open boundary, exits the domain without reflection (radiation condition), the wave, traveling towards the shelf, propagates without change of amplitude. This is because the bottom friction at 3km depth is negligible (T=39min). At T=57.6min, the tsunami impinges on the shelf break resulting in the tsunami splitting into two waves (T=1h16min) due to partial

reflection: a backward traveling wave with amplitude of ~0.5 m, and a forward traveling wave towards the very shallow domain (T=1h27min).

While the wave reflected from the shelf break travels without change of amplitude, the wave on the shelf is strongly amplified. The maximum amplitude attained is
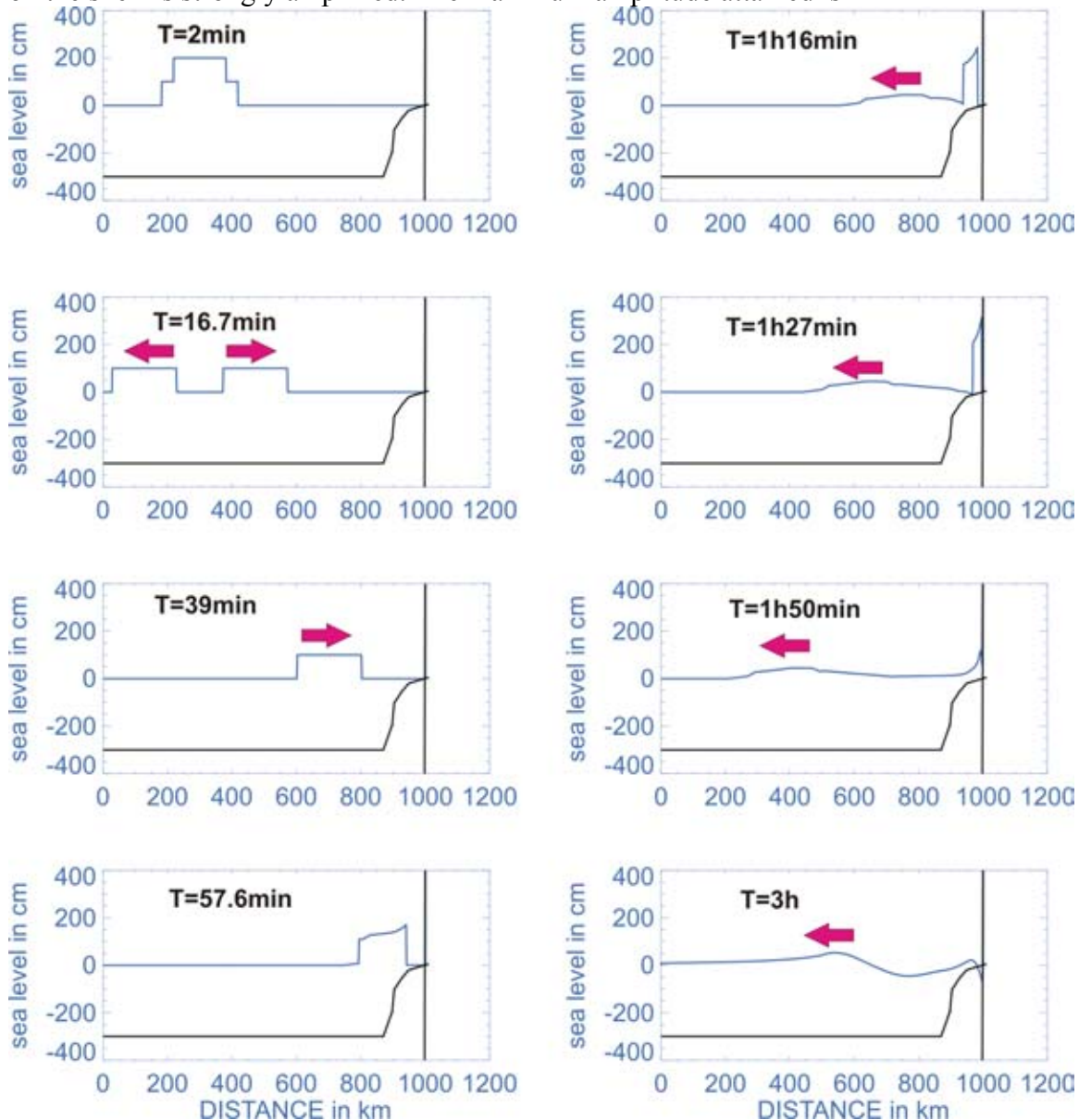

Figure 2. History of tsunami propagation. Generated by the bottom deformation at T=40s this tsunami wave experiences significant transformations and reflections. Black lines denote bathymetry. Vertical line denotes true bathymetry at the tsunami range from -4m to 4m. The second black lines repeats bathymetry from Figure 3, scale is 1:1000.

approximately 7.2m (not shown). Figure 2 (T=3h) shows the time when the wave reflected from the shelf break left the domain and the wave over the shelf oscillates with an amplitude

diminishing towards the open ocean. These trapped and partially leaky oscillations continue for many hours, slowly losing energy due to waves radiating into the open ocean and due to the bottom dissipation. This behavior is also described in Fig. 3, where temporal changes of the sea level and velocity are given at the two locations. At the boundary between dry and wet domain the sea level changes when runup reaches this location. It is interesting to note that repeated pulses of the positive sea level are associated with velocity which goes through the both positive and negative values. At the open boundary the initial box signal of about 20min period is followed by the wave reflected from the shelf break and the semi-periodic waves radiated back from the shelf/shelf break domain. The open boundary signal which is radiated into open ocean, is therefore superposition of the main wave and secondary waves. The period of the main wave is defined by the size of the bottom deformation and ocean depth (initial wave generated by earthquake) while the periods of the secondary waves are defined by reflection and generation of the new modes of oscillations through an interaction of the tsunami waves with the shelf/shelf break geometry.

In numerous publications (e.g. Munk, 1962; Clarke, 1974, Mei, 1989), it was shown that the shelf modes of oscillations usually dominate meteorological disturbances observed along coasts. The evidence for tsunamis trapped in a similar manner have been presented both, theoretically (Abe and Ishii, 1980) and in observations (Loomis, 1966; Yanuma and Tsuji, 1998; Mofjeld et. al., 1999).
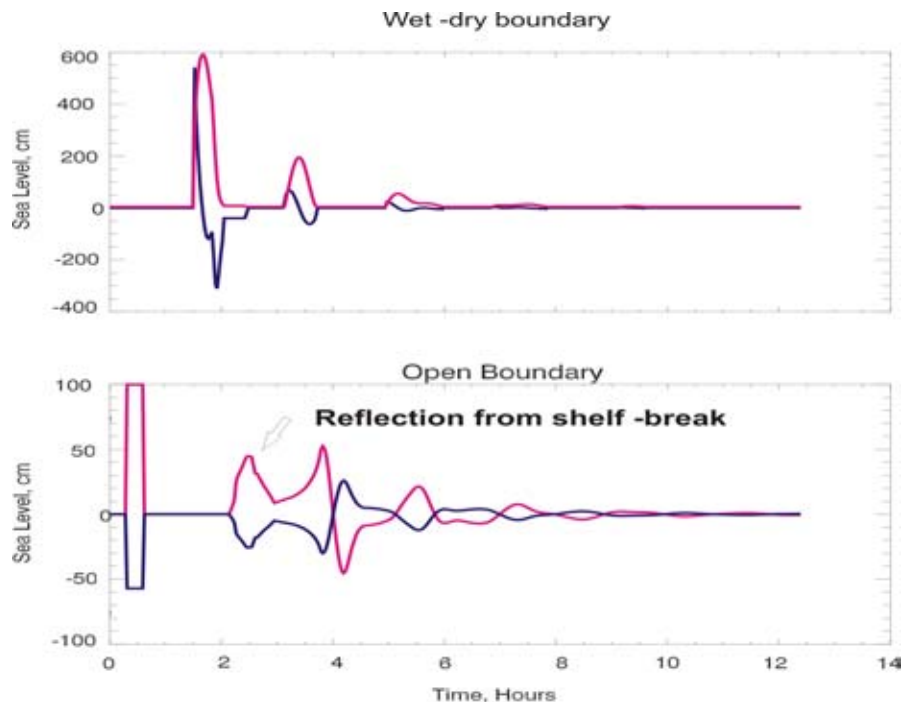

Figure 3. Tsunami temporal change of the sea level (red) and velocity (blue) at the wet-dry boundary (upper panel) and at the open boundary (lower panel). Velocities are expressed in the cm/s, and the lower panel numbers should be divided by 10.

To investigated the tide wave behavior in the same channel we shall introduce into radiating boundary condition (eq. 9) the sea level and velocity in he form given by eq.(10),

$$\zeta_p = 273.19\cos(\omega t - 0.821484) \quad \text{and} \quad u_p = 16.6974\cos(\omega t - 5.53261) \tag{11}$$

Here omega is M_2 tide frequency (see Table 1). As boundary signal is transmitted into domain a stationary solution is obtained after five tidal periods. In Fig. 4 a three tidal period are given to depict tidal periodicity at the open and wet-dry boundaries. The entire solution included 10 periods.
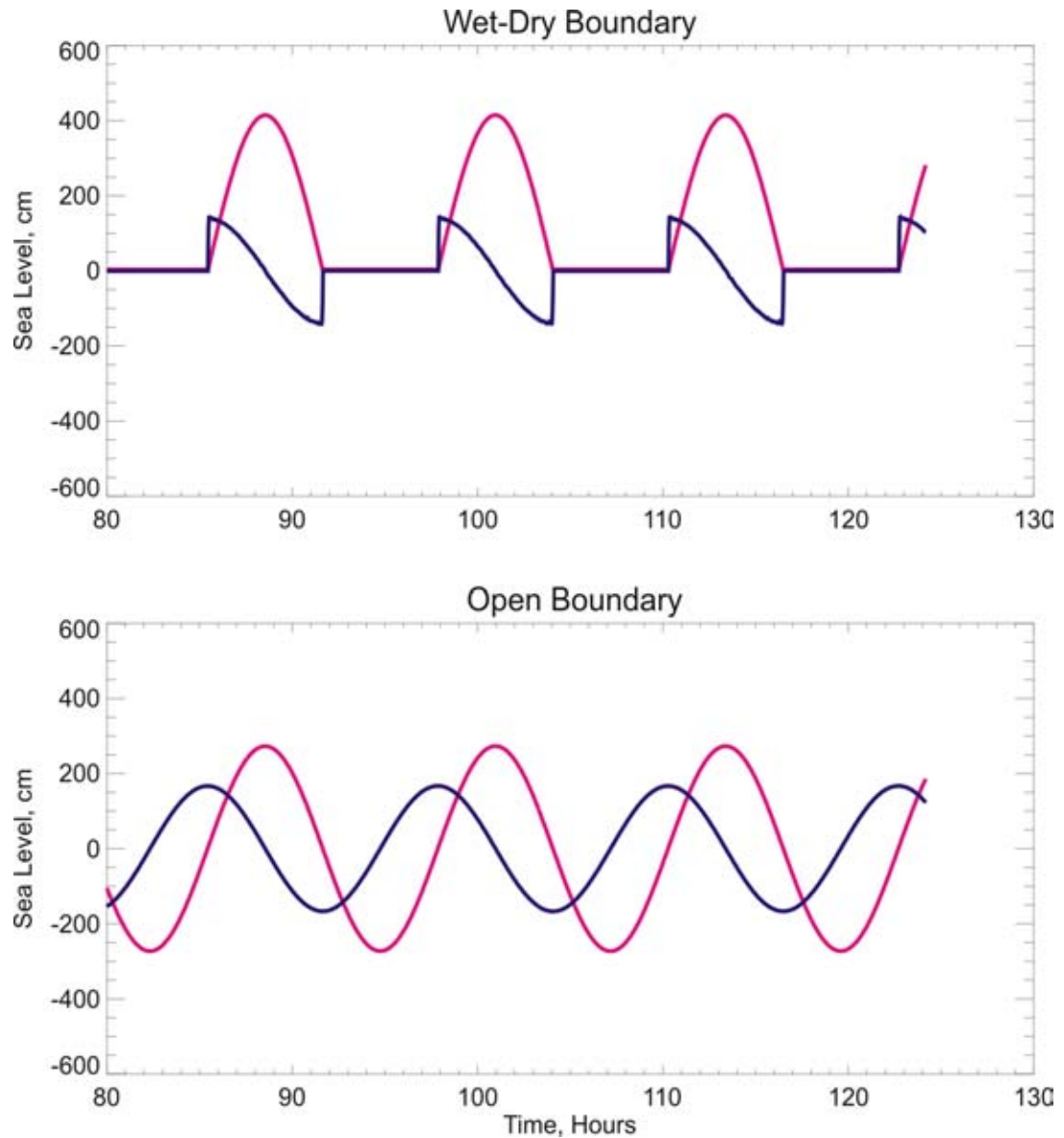

Figure 4. M_2 tide temporal changes: sea level (red) and velocity (blue). Velocities are expressed in the cm/s, and in both panels numbers should be divided by 10.

As one shall expect the tidal signal is periodical in time and space with peculiarities in the region of the wet-dry boundary. The distribution of the tidal velocities and sea level along the channels shows that tide actually generated standing wave (Fig. 5), see Defant

(1960). In Fig. 5 the M_2 sea level and velocity is given along the channel for the four phases of the wave. These phases were chosen in proximity to the minimum, maximum and zero for the sea level and velocity.
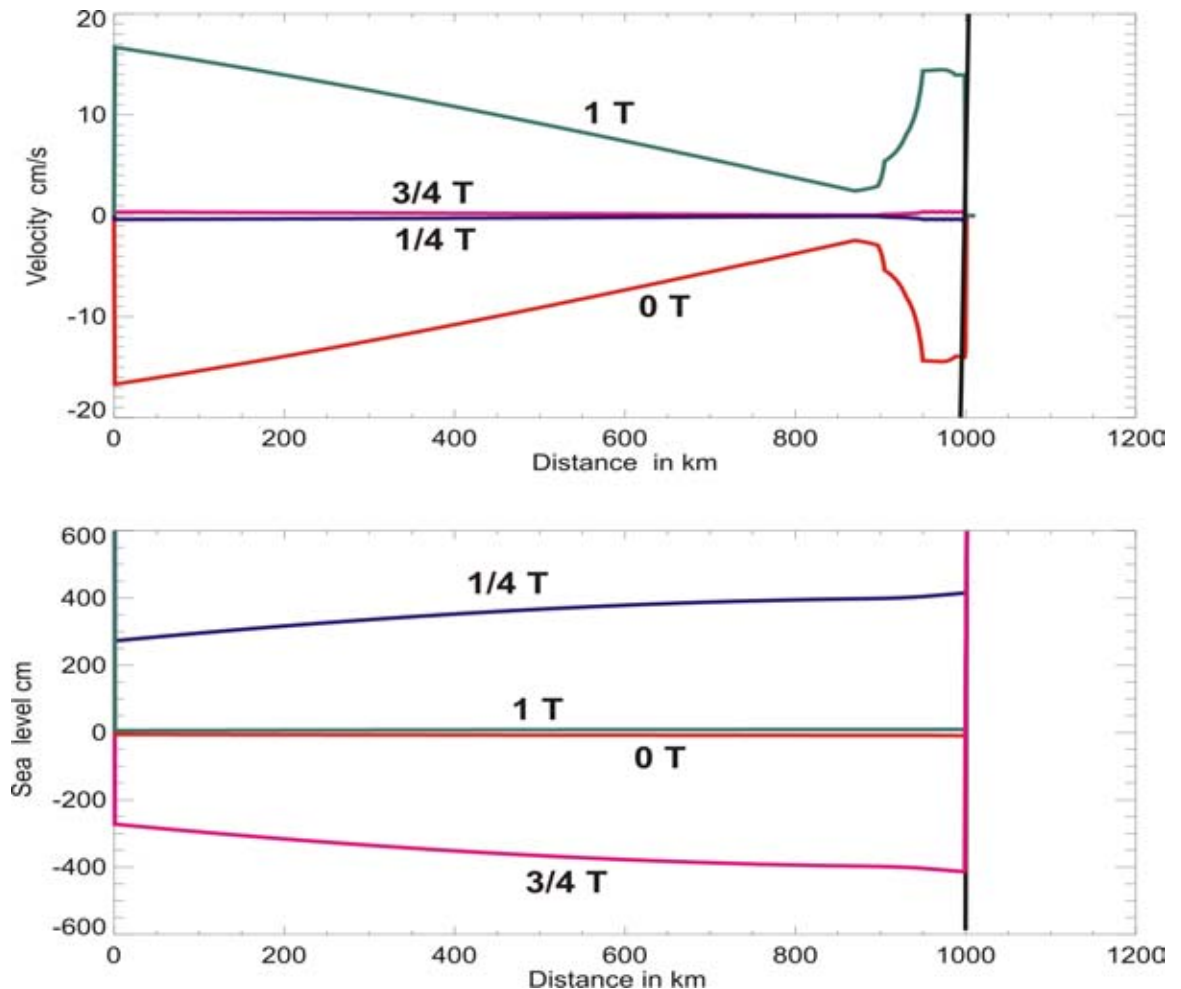

Figure 5. Velocity (upper panel) and sea level (lower panel) of the M2 tide along the channel at the four phases of 12.42 hour cycle.

The maximum or minimum of the sea level (and velocity) is having the same phase from the mouth to the head of the channel. The sea level show steady increase towards the channel's head, while the velocity is more differentiated with the minimum in proximity to the shelf break. The slow change of tidal parameters along the channel is juxtaposed against the faster change of the tsunami parameters with 20min variability generated by the bottom deformation (Fig. 3, lower panel). The resulting tide-tsunami interactions are   described in Fig. 6. The tsunami is generated in such a fashion that it will arrive to the shore when the tidal amplitude achieve maximum. The joint amplitude of tide and in proximity to the wet-

dry boundary is close to 10m (Fig. 6 upper panel). The signal radiated from the domain is given in Fig.6, lower panel. This signal when detided depicts the same tsunami as in Fig. 3 (lower panel). We may conclude that the tides and tsunami propagating in channel from Fig. 1 are superposed in a linear fashion. This is due mainly to the small tidal currents.
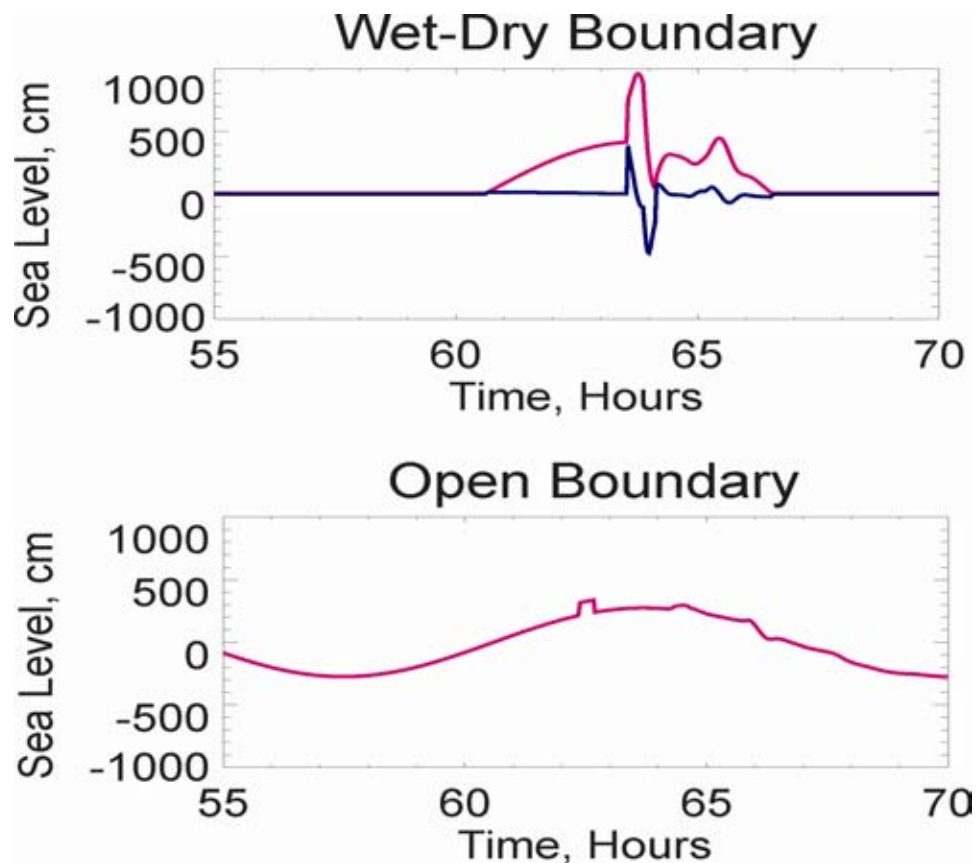

Figure 6. Tsunami and tide temporal change of the sea level (red) and velocity (blue) at the wet-dry boundary (upper panel) and at the open boundary (lower panel).

To elucidate tide/tsunami interaction in the wet-dry region, we superpose the maximum of sea levels and velocities along the channel obtained through the independent computation of tides and tsunami, and tsunami and tides computed as one process given in Fig.6. The last 20km before the wet-dry boundary are shown in Fig. 7. While tide (green color) show very small amplitude increase (upper panel, maximum 415cm) and very small velocity (lower panel, maximum is 16.7cm/s), the tsunami (blue color) is strongly enhanced in both sea level (maximum 721cm) and velocity (maximum 627cm/s). The dry domain starts

at the 1000km and the horizontal runup due to the tide is 980 m and due to the tsunami is 1700m. By adding together the results from the two independent computations (red line) we are able to obtain the distribution of maximum of the sea level and velocity but not a joint runup. Joint computation moves the sea level and velocity into previously dry domain (dashed lines). As in the previous experiment the tidal velocity was relatively very small a nonlinear interaction could occur only for the short time span in the very shallow water where sea level change due to tide and tsunami is of the order of depth.
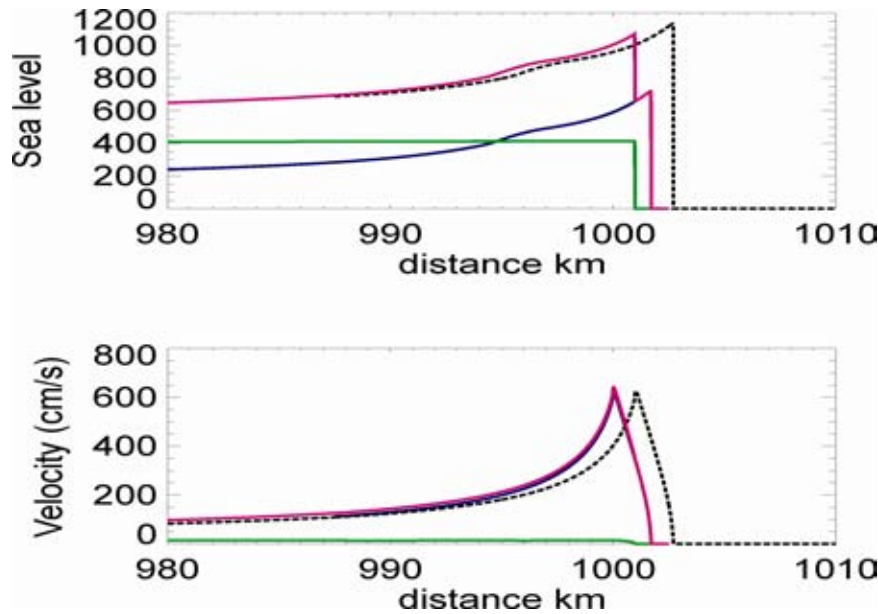

Figure 7. Distribution of the maximum of velocity (lower panel) and sea level (upper panel). Green lines: only tides; blue lines: only tsunami; red lines: superposition of tides and tsunami; dashed lines: joint computation of tides and tsunami.
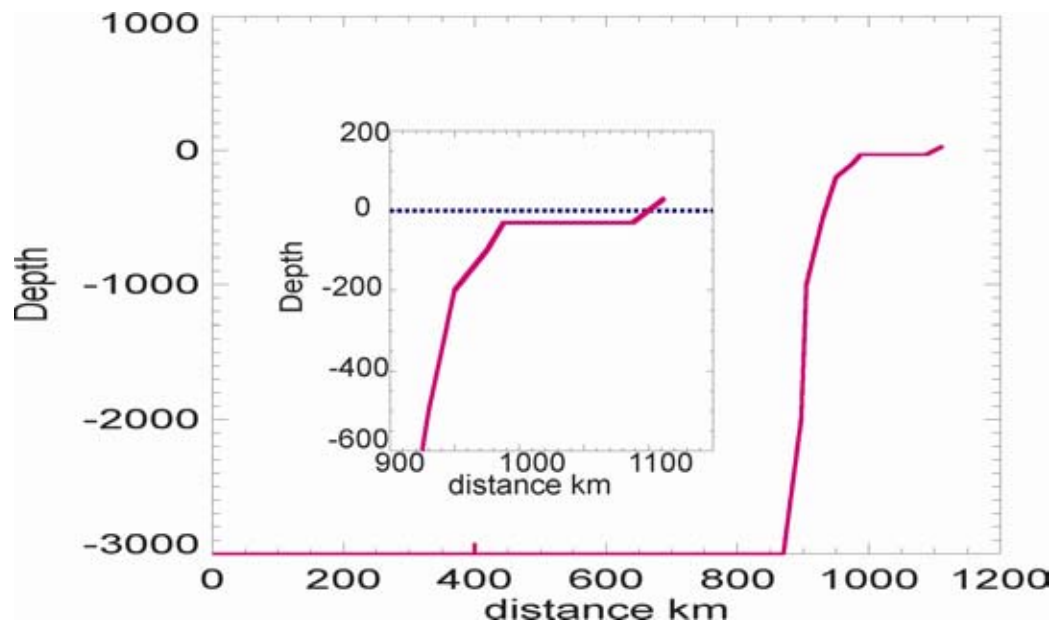
Figure 8. Typical bathymetry profile cutting continental slope and shelf break in the Gulf of Alaska. To imitate shallow water bodies connected to the Gulf a 100km of 30m depth (insert) is added to the profile from Fig. 1.

We consider now a similar depth distribution to the Fig. 1 but to enlarge tidal velocity a shallow channel of the 100km long is introduced between 990km and 1090km (see Fig. 8). This channel imitates the water bodies like Cook Inlet with extended shallow depth and strong transformation of the current.
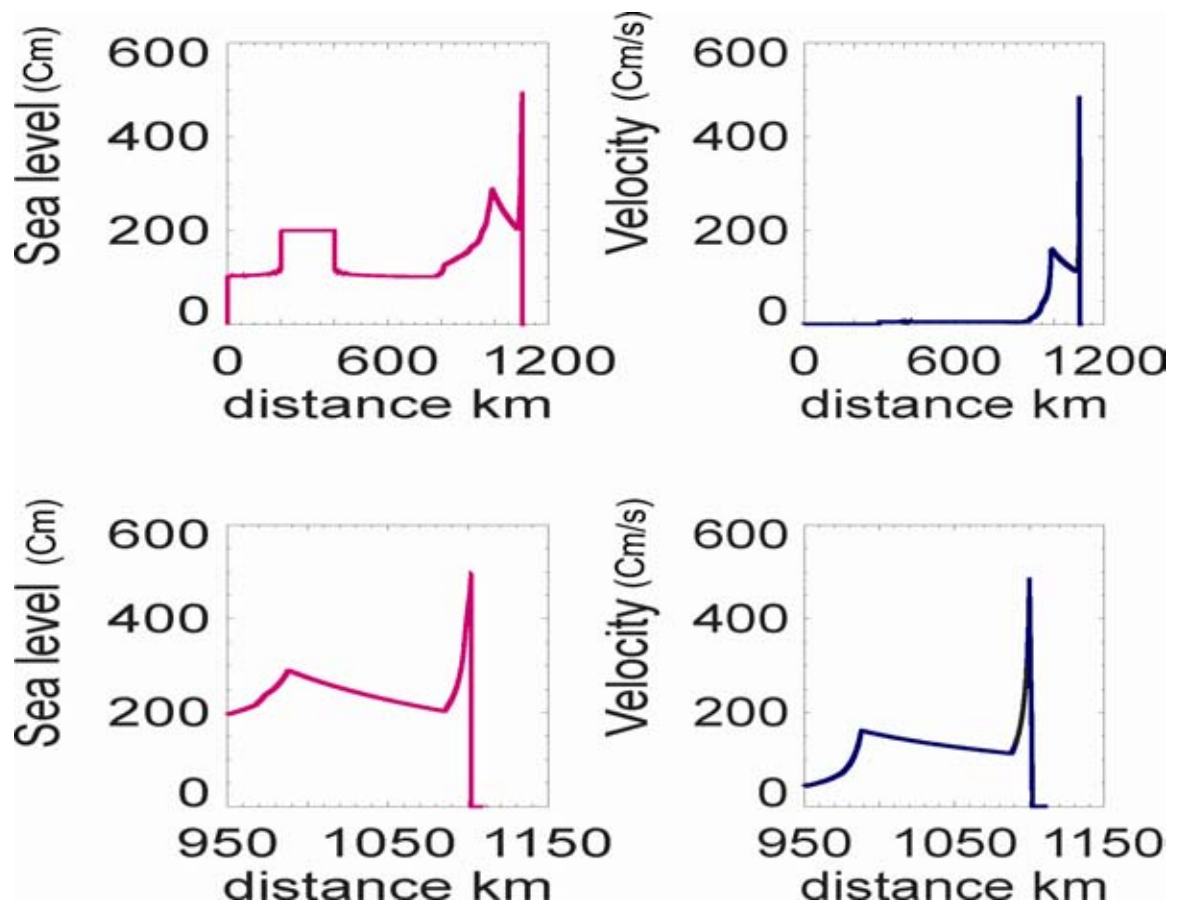
Figure 9. Distribution along the channel of the maximum of tsunami velocity (blue lines)) and tsunami sea level (red lines). Upper panel: along the entire channel. Lower panels: along the shelf.

The results for the computed tsunami are given as distributions of maximum sea level and velocity along the channel (Fig. 9). In tsunami approaching shallow water channel both sea level and velocity are amplified, but this amplification is slowly dissipated along 100km channel due to the bottom friction. Again both velocity and sea level are strongly enhanced on the sloping beach. Maximum current in the sloping beach region is 487cm/s and the sea level increases to 495cm. Thus comparing with the previously considered propagation which resulted in 721cm of the maximum sea level, the strong reduction of the sea level is observed and can be attributed to the shallow water dissipation.
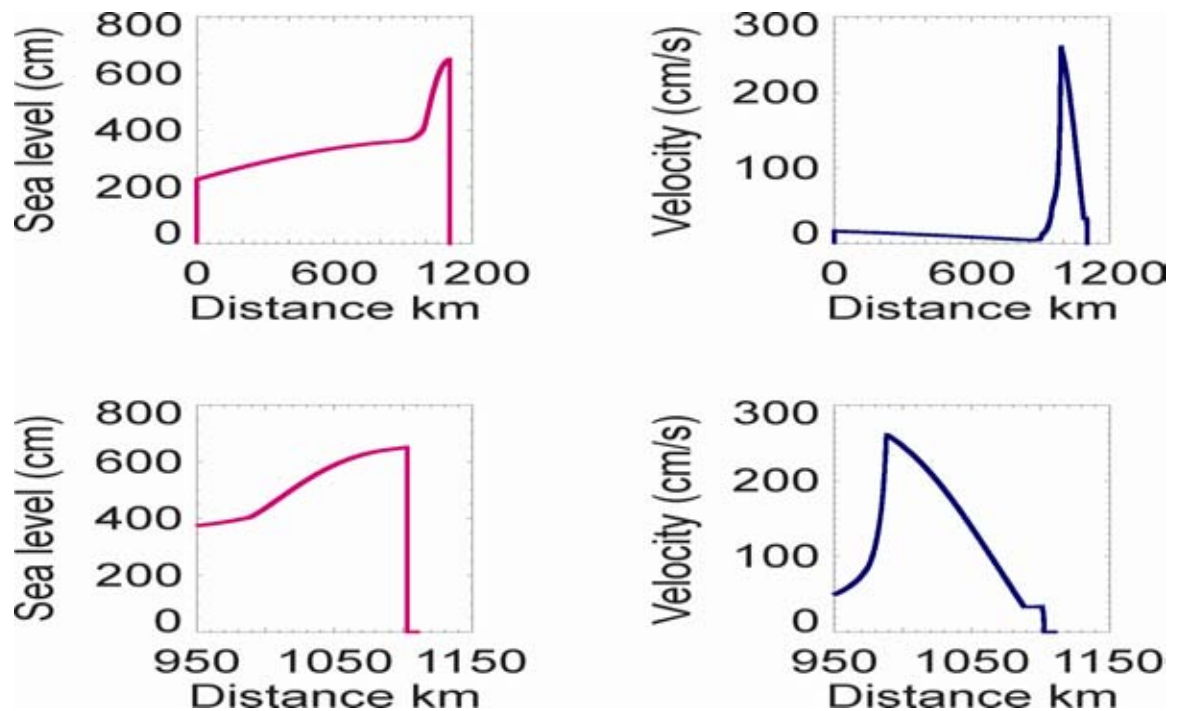The behavior of the M_2 tide is described in the Figure 10.

Figure 10. Distribution along the channel of the maximum of tide velocity (blue lines)) and tide sea level (red lines). Upper panel: along the entire channel. Lower panels: along the shelf.

The tide dynamics along the channel is quite different from the tsunami. Upon entering from the deep ocean into shallow channel both tide and tsunami sea level is amplified. Along the 100km channel the sea level of the tsunami steady diminishes while the tide sea level is steady increasing. On the other hand both tsunami and tide currents are dissipated along the channel. But the most conspicuous difference occurs in the sloping beach portion of the channel. Whereas along the short distance of 10km the tsunami current and sea level is amplified about 2-3 times, the tidal sea level is showing a few cm increase and tidal current is constant along this shallow water. The relatively large tidal (apr. 260cm/s) and tsunami (apr. 160cm/s) velocity in the shallow channel may reasonably be assumed as the primary source of the nonlinear interactions between tide and tsunami.

In the joint tsunami/tide signal (Fig. 11) two regions of enhanced currents have been generated; one at the entrance to the shallow water channel where tidal current dominates and the second at the beach where tsunami current dominates. The nonlinear interactions have been elucidated in Fig. 11. While superposed signal of tide and tsunami (red lines) and jointly computed tide and tsunami (dash black lines) are the same in the deep water channel, they diverge in the shallow water channel. Both sea level and velocity in the joint computation have smaller values than the signal obtained by superposition. We may conclude that the joint signal has been reduced due to tide/tsunami nonlinear interaction.
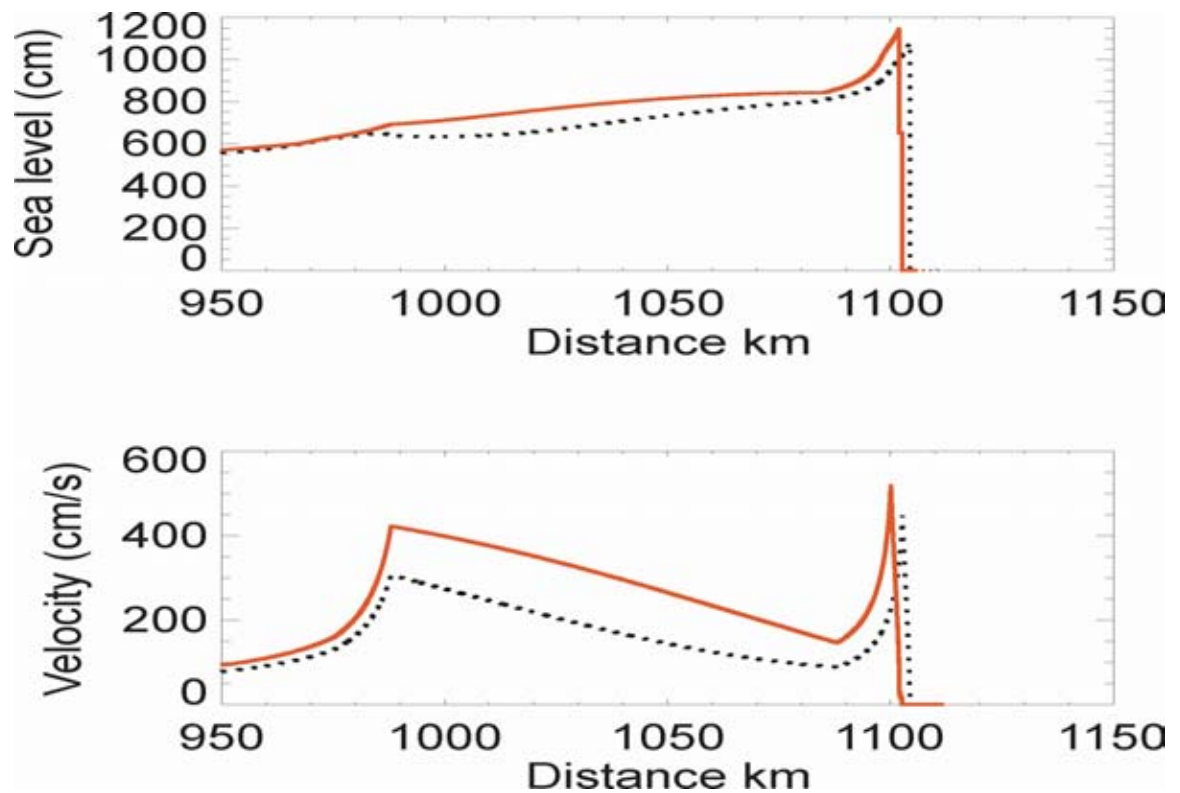
Figure 11. Distribution of the maximum of velocity (lower panel) and sea level (upper panel) in the shallow part of the channel. Red lines: linear superposition of tides and tsunami simulated separately; dashed lines:show results for tides and tsunami simulated together and resulted in their non-linear interaction.

3. DISCUSSION AND CONCLUSION.

Two simple cases of tide/tsunami interactions along the narrow and wide shelf have been investigated to define importance the nonlinear interactions. In a channel with narrow shelf the time for the tide/tsunami interactions is very short and mainly limited to the large currents in the runup domain. In the channel with extended shallow water region the nonlinear bottom dissipation of the tide and tsunami leads to strong reduction in tsunami amplitude and tsunami currents. The tidal currents and amplitude remain unchanged through interaction with tsunami. The main difference in behavior of tide and tsunami is related to the wave length, while M_2 tide in the 3km deep ocean has wavelength of 7670km, the wavelength of 20min period tsunami is only 206km. The 100km shallow water channel is a half-wavelength for tsunami but only 1.3% of the tide wavelength. The major difference between tide and tsunami occurs in the runup region. Tide does not undergo changes in the velocity or sea level in the nearshore/runup domain while for tsunami this is the region of major amplification of the seal level and currents.

In summary, the energy of an incident tsunami can be redistributed in time and space with the characteristics which differ from the original (incident) wave. These changes are induced by the nonlinear shallow water dynamics and by the trapped and partially leaky oscillations controlled by the continental slope/shelf topography. The amplification of

tsunami amplitude is mainly associated with strong amplification of tsunami currents. The nonlinear interaction of the tide with tsunami is important, as it generates stronger sea level change and even stronger changes in tsunami currents, thus the resulting run-up ought to be calculated for the tsunami and tide propagating together.

REFERENCES:

Abe, K. and Ishii, H. 1980. Propagation of tsunami on a linear slope between two flat regions. Part II reflection and transmission, J. Phys. Earth, 28, 543-552.

Clarke, D. J. 1974. Long edge waves over a continental shelf, Deutsche Hydr. Zeit., 27, 1, 1-8.

Defant, A., 1960. Physical Oceanography, Pergamon Press, v 2, 598pp.

Durran, D. R. 1999. Numerical Methods for Wave Equations in Geophysical Fluid Dynamics, Springer, 465pp.

Flather, R.A. 1976. A tidal model of the north-west European continental shelf. Mem. Soc. R. Sci. Lege, 6, 141-164.

Kowalik, Z. 2003. Basic Relations Between Tsunami Calculation and Their Physics - II, Science of Tsunami Hazards, v. 21, No. 3, 154-173

Kowalik Z., W. Knight, T. Logan, and P. Whitmore. 2005a. NUMERICAL MODELING OF THE GLOBAL TSUNAMI: Indonesian Tsunami of 26 December 2004. Science of Tsunami Hazards, Vol. 23, No. 1, 40- 56.

Kowalik, Z., and A. Yu. Proshutinsky, 1994. The Arctic Ocean Tides, In: The Polar Oceans and Their Role in Shaping the Global Environment: Nansen Centennial Volume, Geoph. Monograph 85, AGU, 137--158.

Loomis, H. G. 1966. Spectral analysis of tsunami records from stations in the Hawaiian Islands. Bull. Seis. Soc. Amer. 56, 3 697-713.

Mei, C. C. 1989. The Applied Dynamics of Ocean Surface Waves, World Scientific, 740 pp.

Mofjeld, H.O., V.V. Titov, F.I. Gonzalez, and J.C. Newman (1999): Tsunami wave scattering in the North Pacific. IUGG 99 Abstracts, Week B, July 26–30, 1999, B.132.

Munk, W. H. 1962. Long ocean waves, In: The Sea, v. 1, Ed. M. N. Hill, InterScience Publ., 647-663.

Weisz, R. and C. Winter. 2005. Tsunami, tides and run-up: a numerical study, Proceedings of the International Tsunami Symposium, Eds.: G.A. Papadopoulos and K. Satake, Chania, Greece, 27-29 June, 2005, 322.

Pugh, D. T.. 1987. Tides, Surges and Mean Sea-Level, John Wiley & Sons, 472pp.

Yanuma, T. and Tsuji Y. 1998. Observation of Edge Waves Trapped on the Continental Shelf in the Vicinity of Makurazaki Harbor, Kyushu, Japan. Journal of Oceanography, 54, 9 -18.